Contents lists available at SciVerse ScienceDirect

CIRP Annals Manufacturing Technology

Journal homepage: www.elsevier.com/locate/cirp

Influence of rotary axis angular positioning error motions on robotic probing

S. Ibaraki (2)[a,*], K. Masamine[a], M. Hamamura[b], O. Takahara[b]

a Graduate School of Advanced Science and Engineering, Hiroshima University, Kagamiyama 1-4-1, Higashi-Hiroshima 739-8527, Japan
b Renishaw K.K., 29-8 Yotsuya 4-chome, Shinjuku-ku, Tokyo 160-0004, Japan

The accuracy of touch-trigger probing by a six-axis robotic manipulator is determined by the accuracy of the robot forward kinematic model to estimate the stylus sphere position from angular positions of rotary axes. Many conventional studies have employed the Denavit–Hartenberg (DH) model, containing position and orientation errors of the rotary axis average lines as error sources. This paper proposes the application of a new kinematic model, containing the angular positioning deviations of all the rotary axes, to the robotic probing. The probing accuracy is experimentally investigated in profile probing of a straightedge over the robot's workspace.

Robot, Probe, Accuracy

1. Introduction

A conventional coordinate measuring machine (CMM) is typically in a room under strict thermal control, which continuously consumes significant amount of energy. For some metrological applications in manufacturing, "inline" measurement, performed in or near manufacturing sites, can be an energy- and cost-effective alternative [1]. Ostrowska et al. [2] categorized inline measurement systems into the ones with and without the fixed kinematic constraints. Tactile probing typically has smaller measurement uncertainty than optical methods, and its instrumental cost is often lower. While the tactile probing on a machine tool and an in-line CMM are more popular, the probing by a robotic manipulator potentially has a strong advantage. The portability, with a larger workspace compared to its foot print, is its inherent advantage. Potentially, the probing can be performed by a robot installed on an automated guided vehicle [3].

A touch-trigger probe, widely adopted on machine tools, gives a binary signal as a result of contact with a surface being measured (called a "switching probe" in ISO 230-10 [4]). When a robot controller receives this signal, the angular positions of rotary axes, measured by a rotary encoder, are logged, which give the stylus sphere center position based on the robot forward kinematic model. Therefore, any error in the forward kinematic model results in the measurement error. The review paper [5] reported that the positioning error of commercially available six-axis robots is typically 0.5 to 10 mm, when no compensation is applied. This is not sufficient accuracy required in typical probing applications in manufacturing. As a result, there has been so far very few industrial implementation of the robotic probing.

Few research works have studied the accuracy of robotic probing. Pioneering works by Ostrowska et. al [2][6] employed the artificial neural network (ANN) to improve the accuracy of the robot forward kinematic model. Numerous researchers have studied a model-based compensation to improve the positioning accuracy of six-axis robots, and in principle, these models can be straightforwardly applied to robotic probing. As is reviewed in [5], the majority of these works is based on the Denavit-Hartenberg (DH) model. The DH model, first proposed in 1955 [7], is the most primitive and extremely popular robot kinematics model. Essentially, the DH model contains the errors in the position and orientation of the rotary axis average lines. The *axis average line* of a rotary axis, defined in ISO 230-1 [8], is a line representing the mean position and orientation of the axis of rotation over the entire rotation.

Therefore, the DH model cannot describe an error that changes with the rotation. For machine tools, such angle-dependent errors are referred to as *error motions* [8]. Extending the DH model, the authors' group has proposed a new kinematic model containing the angular positioning deviation (APD) of all the rotary axes. In a robot, the angular positioning error motion is typically caused by tooth-to-tooth variations in the gear pitch error or the elastic deformation of the gear. Therefore, it is generally angle-dependent. The new model was first proposed to a planar robot arm (identified by a tracking interferometer [9] and a laser interferometer [10]) and then extended to a six-axis manipulator [11] (Ref. [12] also considered the axis-to-axis crosstalk). It was further extended to an articulated arm CMM [13]. An analogous kinematic model with error motions was also presented in [14].

This paper's original contribution is on the application of this model to the robotic touch-trigger probing. As reviewed above, very few research works have reported the accuracy of robotic probing. In particular, to the authors' knowledge, no work has studied its accuracy in profile probing, not in point-to-point length measurement. This work experimentally investigates the accuracy in profile probing, taking a straightedge of the length 1,000 mm as the measured object. Then, experiments will show that the conventional DH model cannot show sufficient prediction accuracy of the probing error in the straightness measurement, and that the APDs of rotary axes, included in the proposed model, have a significant influence on the probed profiles.

2. Proposed kinematic model of robotic probing

2.1 Conventional DH model for robotic probing

This study considers the six-axis robot configuration shown in Fig. 1. Since the model proposed in [11] is the basis of this work, this subsection first briefly reviews the conventional DH model, and then Section 2.2 reviews the proposed model in [11].

When the probe detects the contact of the stylus sphere to the target surface, suppose that the angular position of A_n-axis (n=1, .., 6), measured by a rotary encoder, is given by $\theta_n(k) \in \Re$ (k is the point index number). Define: $\Theta(k) = [\theta_1(k), \cdots, \theta_6(k)]$.Then, the stylus sphere center position in the reference coordinate

system (CS), denoted by ${}^{r}\hat{p}(k)\in\Re^3$ (the left-hand side superscript represents the CS) is given by:

$$\begin{bmatrix} {}^{r}\hat{p}(k) \\ 1 \end{bmatrix} = {}^{r}T_6 \cdot \begin{bmatrix} {}^{6}p \\ 1 \end{bmatrix} \quad (1)$$

$$\begin{aligned} {}^{r}T_6 &= {}^{r}T_1 \cdot {}^{1}T_2 \cdot {}^{2}T_3 \cdot {}^{3}T_4 \cdot {}^{4}T_5 \cdot {}^{5}T_6 \quad (2)\\ {}^{r}T_1 &= D_c(\theta_1(k)) \\ {}^{1}T_2 &= D_x(L_{1x}+\delta x_{21})D_z(L_{1z})D_a(\alpha_{21})D_b(\theta_2(k)+\Delta\theta_{20}) \\ {}^{2}T_3 &= D_z(L_{2z}+\delta x_{32})D_a(\alpha_{32})D_c(\gamma_{32})D_b(\theta_3(k)+\Delta\theta_{30}) \\ {}^{3}T_4 &= D_z(L_{3z}+\delta z_{43})D_y(\delta_{y43})D_c(\gamma_{43})D_a(\theta_4(k)+\Delta\theta_{40}) \\ {}^{4}T_5 &= D_x(L_{4x}+\delta x_{54})D_z(\delta z_{54})D_c(\gamma_{54})D_b(\theta_5(k)+\Delta\theta_{50}) \\ {}^{5}T_6 &= D_z(L_{5x})D_z(\delta z_{65})D_y(\delta y_{65})D_c(\gamma_{65})D_a(\theta_6(k)) \end{aligned}$$

where ${}^{6}p\in\Re^3$ is the position of the stylus sphere in the A_6-axis CS. $D_*(\dagger)\in\Re^{4\times4}$ denotes the homogeneous transformation matrix (HTM) representing the linear translation to the X-, Y-, and Z-directions (for *: x, y, z) by the distance $\dagger\in\Re$, or the rotation around the X-, Y-, and Z-axes (for *: a, b, c) by the angle †. Their formulation is given in [15]. $L_*\in\Re$ represent the nominal link lengths. The other 18 parameters, for example, δx_{21}, α_{21}, $\Delta\theta_{20}$, ..., are the D-H parameters. See [15] for their definitions.

2.2 Inclusion of angular positioning deviations

Typically, a rotary encoder measures the angular position of the motor axis. Due to e.g. the gear transmission error, actual angular position of its driving shaft can deviate from it. The proposed model [11][12] assigns the APD, represented by $\Delta\theta^{\square}_{n,map}(i_n,\pm1)$, for the prescribed set of A_n-axis nominal angular positions, $\theta_{n,map}{}^*(i_n)\in\Re$, where $i_n\in\Re$ is the index number (i_n=1, ..., N_n), and for the rotating direction (+1 or -1). In other words, the APD is modeled in a lookup table with the nominal angular position and rotation direction as inputs.

When the A_n-axis angle, $\theta_n(k)$, is measured by a rotary encoder, its actual angular position is estimated by linearly interpolating $\Delta\theta^{\square}_{n,map}(i_n,\pm1)$. Then, the end effector position, ${}^{r}\hat{p}(k)$, can be estimated by replacing $\theta_n(k)$ in the model (1) with it.

In [11][12], we also presented a scheme to measure the APDs, $\Delta\theta^{\square}_{n,map}(i_n,\pm1)$ (i_n=1, ..., N_n) of the A_n-axis, as well as all the DH errors. As illustrated in Fig. 2, each rotary axis is indexed at the prescribed set of command angular positions, and the three-dimensional (3D) position of the retroreflector, attached to the robot's end effector, is measured by using a tracking interferometer.

3. Experimental investigation of probing accuracy

3.1 Experimental setup

The objective is to experimentally investigate the accuracy of the robotic probing, comparing the cases where the nominal and proposed kinematic models are used. The probing accuracy can significantly depend on the measurement location in the robot workspace. To investigate this influence, probing tests are performed at total six different locations.

Figure 1 shows the experimental setup. A six-axis robot, KUKA KR30HA (rated payload: 30 kg) was used. A touch-trigger probe, RMP-400 by Renishaw, was installed to its end effector flange (major specifications in the manufacturer's catalog: Unidirectional repeatability (2σ): 0.35 μm for stylus length 100 mm, 3D pre-travel variation in X, Y, Z: ±1.75 μm for stylus length 100 mm).

A straightedge, made of gabbro stone, was probed. As shown in Fig. 3, total 100 points were probed over 1,000 mm on its side and top faces with a constant interval, 10 mm. The stylus direction is regulated in the Z-direction (see Fig. 1). The A6-axis is regulated so that the approaching direction is always the same with respect to the probe orientation. This makes the influence of the probe's pre-travel variation [4] negligibly small.

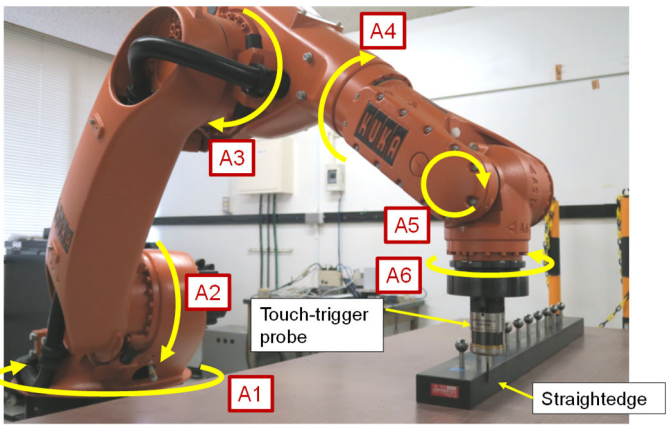

Figure 1. Robot configuration and touch-trigger probing setup

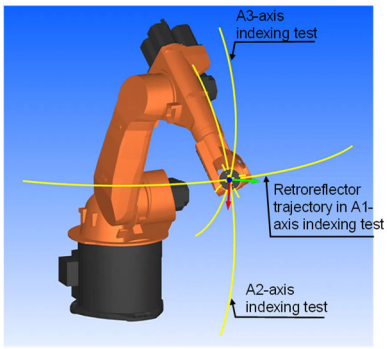

Figure 2. Axis indexing tests for the identification of the proposed model

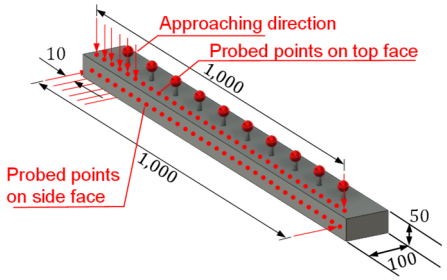

Figure 3. Probed points on the straightedge (spheres were not probed)

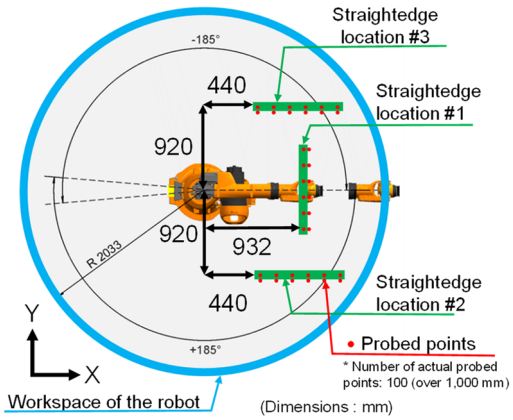

Figure 4. Locations of the straightedge in robot workspace

In advance, actual straightness profiles of the faces were measured by a CMM. Both faces have the straightness error sufficiently small compared to the robot's positioning accuracy (< 3 μm on the side face, and <8 μm on the top face). The straightedge was placed at Locations #1 to #3 shown in Fig. 4. The straightedge was put on a table without any clamping.

First, the repeatability of the robotic probing was investigated by repeatedly probing the same point on the side face (probing to –X

direction) and the top face (probing to –Z direction) of the straightedge. Each test approximately took 90 sec. Table 1 shows the range (max - min) of the probed positions. Total three tests were performed at 30 and 165 min from the first test. The variations in the probed positions is mostly attributable to the robot's positioning repeatability error, including the thermal influence within 90 sec. Smaller variation at 165 min may be because the robot reached closer to the thermal equilibrium.

3.2 Prediction of probing error profiles by the proposed model

First, the axis indexing tests, depicted in Fig. 2, were performed to identify the proposed model. Figure 5 shows the identified APDs of A1- and A2-axes, $\Delta\theta^{\square}_{\mathrm{n,map}}(i_n, \pm 1)$ (i_n=1, ..., N_n) (n=1, 2). A3- to A6-axis APDs were also identified, as well as 18 DH errors.

Refer the kinematic model, given in Eq. (1), to as the *nominal model*, $f_{\mathrm{nominal}}(\Theta(\mathrm{k}))$, when it contains no error parameter. In the conventional probing with the nominal model, when the rotary axis angular positions, $\Theta(k)$, are logged, the stylus sphere position, ${}^{\square}_{r}\hat{p}_{\mathrm{nominal}}(k)$, is estimated by:

$$ {}^{\square}_{r}\hat{p}_{\mathrm{nominal}}(k) = f_{\mathrm{nominal}}(\Theta(k)) \tag{3} $$

An error in the nominal model causes an error in the probed stylus sphere position. In this section, this probing error is predicted by using the proposed model and is compared to actual probing error profile.

Since the geometric error of the straightedge is negligibly small, the probed points, ${}^{\square}_{r}p^{*}(k)$ (k=1, ..., N), can be estimated by linearly interpolating the first and last points. Denote the kinematic model (1) as the *proposed model*, $f_{\mathrm{proposed}}(\Theta(k))$, containing the identified DH errors and APDs of all the axes. By inversely solving it, angular positions of all the axes for ${}^{\square}_{r}p^{*}(k)$ can be simulated:

$$ \hat{\Theta}(k) = f^{-1}_{\mathrm{proposed}}({}^{\square}_{r}p^{*}(k)) \tag{4} $$

Then, when the nominal model is applied, the probing error profile can be simulated by:

$$ {}^{\square}_{r}\hat{p}_{\mathrm{predicted}}(k) = f_{\mathrm{nominal}}(\hat{\Theta}(k)) \tag{5} $$

Figure 6 compares the predicted stylus sphere trajectory, ${}^{\square}_{r}\hat{p}_{\mathrm{predicted}}(k)$ (in black) with its actual measurement, ${}^{\square}_{r}\hat{p}_{\mathrm{nominal}}(k)$, calculated by Eq. (3) with the measured A1- to A6-axis angular positions (in blue). For further comparison, the green profile shows the predicted profile, ${}^{\square}_{r}\hat{p}_{\mathrm{predicted,DH}}(k)$, when the kinematic model contains the DH errors only.

It is clear that the conventional DH model cannot show sufficient prediction accuracy. The proposed model shows significantly better match with the measured profile. This illustrates a significant influence of the rotary axis angular positioning error motions on the profile probing. Since the prediction performance of the proposed model is validated, it will be applied to improve the probing accuracy in the following subsection.

3.2 Improvement of probing accuracy by the proposed model

From the rotary axis angular positions, $\Theta(k)$, logged at the moment of contact, the stylus sphere position, ${}^{\square}_{r}\hat{p}_{\mathrm{proposed}}(k)$, can be estimated by the proposed model:

$$ {}^{\square}_{r}\hat{p}_{\mathrm{proposed}}(k) = f_{\mathrm{proposed}}(\Theta(k)) \tag{6} $$

Figure 7 a-1) and b-1) compare the probed trajectories based on the proposed model (in black), ${}^{\square}_{r}\hat{p}_{\mathrm{proposed}}(k)$, with the one based on the nominal model (in blue), ${}^{\square}_{r}\hat{p}_{\mathrm{nominal}}(k)$. Figure 7 a) shows the probed points on the side face of the straightedge at Location #1, and b) shows those on the top face at Location #1.

Table 1 Range of the probed positions when the same point on the straightedge was probed ten times repeatedly (duration: 90 sec).

	#1 (at 0 min)	#2 (at 30 min)	#3 (at 165 min)
Range (probing to –X direction)	14 μm	20 μm	5 μm
Range (probing to –Z direction)	4 μm	4 μm	3 μm

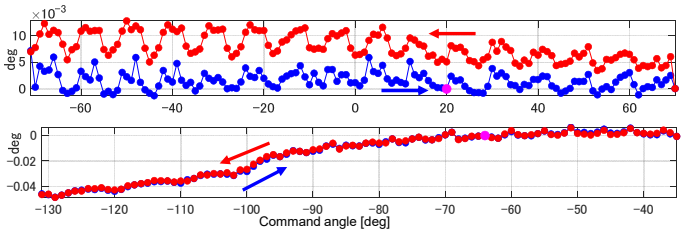

Figure 5. Identified APDs of a) A1-, and b) A2-axes. Red and blue profiles are for positive and negative directions.

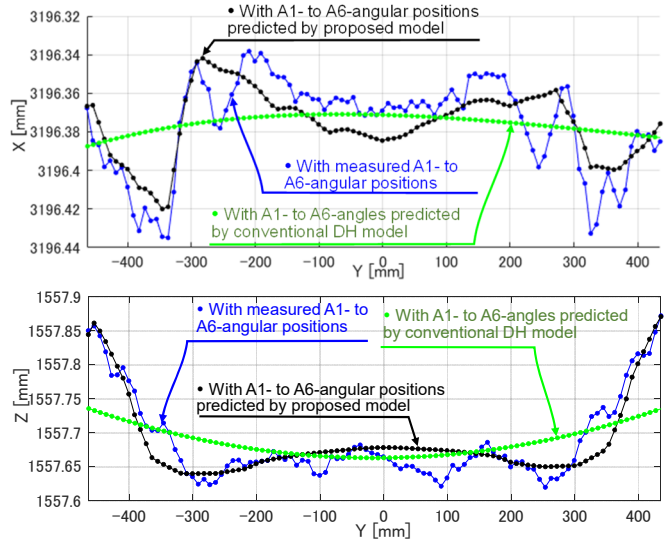

Figure 6. Predicted stylus sphere profile, ${}^{\square}_{r}\hat{p}_{\mathrm{predicted}}(k)$, by the proposed model (in black), the predicted profile, ${}^{\square}_{r}\hat{p}_{\mathrm{predicted,DH}}(k)$, by the conventional DH model (in green), and its actual measurement, ${}^{\square}_{r}\hat{p}_{\mathrm{nominal}}(k)$, calculated by measured A1- to A6-axis angles (in blue). a) Side face on the straightedge location #1, b) top face on location #1.

Since the actual straightness error of the target faces is negligibly small, the probed deviations in Fig. 7 show the probing error. In the histograms, the nominal model (in blue) gave approximately 1.0 mm probing error (max – min) on the side surface and 2.5 mm on the top surface. Figure 7 a-2) and b-2) clearly shows that the conventional DH model gave very small improvement in the probing accuracy. On the other hand, the proposed model significantly reduces the probed deviations.

Table 2 summarizes the standard deviation of the probed displacements, and the straightness error, i.e. the difference between the maximum and minimum displacements, as indices pf the probing error. Compared to the nominal model, the proposed model reduced the probing error by 38% at minimum, and 58% at maximum, in the straightness.

Finally, to compare with the measuring performance of a tracking interferometer, which is more widely used for in-line geometric measurement, Fig. 8 shows the straightness profile of the side face measured by using a tracking interferometer (Leica AT960-XR). A probe with a retroreflector was contacted with the side face at approximately every 100 mm by a human operator. Figure 8 shows that its measurement error did not differ much from the robotic probing with the proposed model (Fig. 7 and Table 2). This illustrates a potential performance of the automated robotic probing.

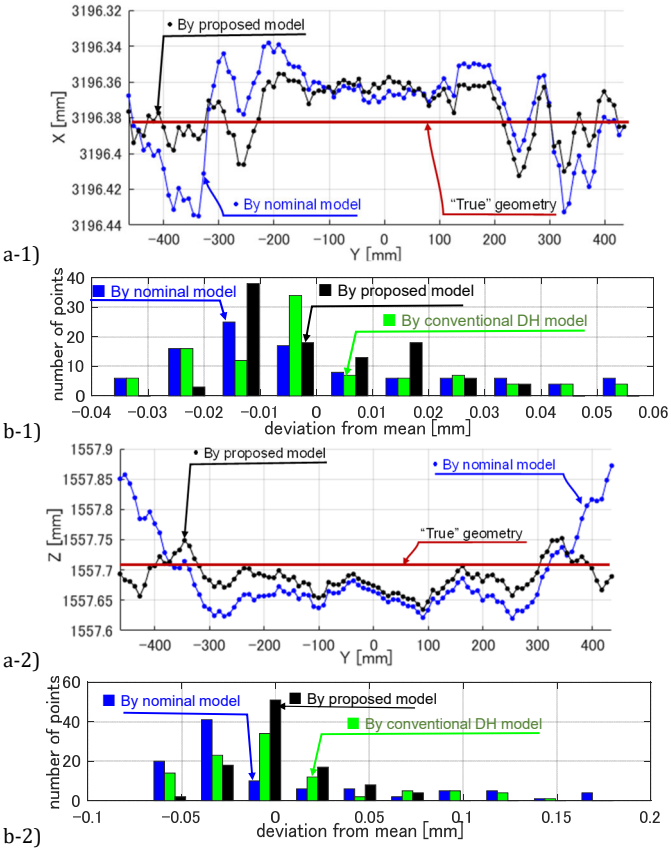

Figure 7. a-1) and a-2) Probed positions calculated with the nominal model (blue) and the proposed model (black). b-1) and b-2) Histograms of the deviations. a) side face at Location #1. b) top face at Location #1.

Table 2 Comparison in standard deviation (Std. dev.) and straightness error (max-min) of the probed profiles

	By nominal model	By conventional DH model	By proposed model	Reduction of probing error by proposed model
Location #1, side face				
Std. dev.	24.6 μm	22.0 μm	14.9 μm	40 %
Straightness	96.7 μm	91.5 μm	56.9 μm	41 %
Location #1, top face				
Std. dev.	62.9 μm	45.9 μm	24.4 μm	61%
Straightness	252.2 μm	205.5 μm	117.6 μm	53%
Location #2, side face				
Std. dev.	30.4 μm	28.9 μm	19.6 μm	36 %
Straightness	142.0 μm	135.9 μm	88.6 μm	38 %
Location #2, top face				
Std. dev.	47.1 μm	34.9 μm	37.1 μm	21 %
Straightness	258.8 μm	203.7 μm	157.9 μm	39 %
Location #3, side face				
Std. dev.	37.3 μm	40.4 μm	14.4 μm	61 %
Straightness	154.1 μm	193.3 μm	65.3 μm	58 %
Location #3, top face				
Std. dev.	59.6 μm	47.3 μm	42.0 μm	30 %
Straightness	327.4 μm	280.4 μm	167.3 μm	49 %

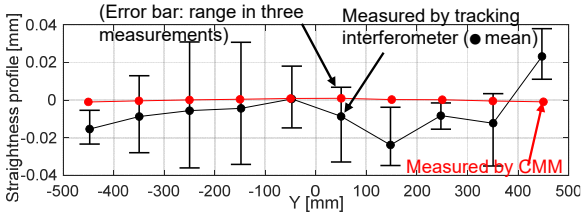

Figure 8. Straightness profile of the side face of the straightedge measured by using a tracking interferometer.. The measurement was repeated three times, and the mean values (black dots) and ranges (in error bars) are shown. Red dots represent the "true" profile measured by a CMM.

4. Conclusion

Due to typically very large positioning error of a six-axis robot, compared to the demanded measurement accuracy, there has been so far very few industrial implementation of the robotic probing. Contributions of this paper can be summarized as follows:

- The new kinematic model, containing the APDs of all the rotary axes, was applied to calculate the stylus sphere position.
- Experiments showed that the conventional DH model did not significantly improve the accuracy of profile probing. The APDs have significant influence.
- Experiments showed that the proposed model reduced the probing error by 38% to 58% in the straightness, compared to the nominal model.

The improvement achieved by applying the present model was notable, but there is still a significant error. Potential uncertainty contributors include a modelling error of the backlash in each rotary axis, the posture-dependent elastic deformation due to the gravity [12], thermal influence [16], and rotary axis error motions other than the angular positioning error motion.

This paper only studied the straightness measurement, because the influence of rotary axis error motions can be observed clearly in such a profile measurement. In our near-future research, we will extend this study to more general dimensions and forms, including point-to-point lengths and 3D geometries.

Acknowledgement

This work was supported in part by JSPS KAKENHI (JP 21H01228).

References

[1] Mutilba U, Gomez-Acedo E, Kortaberria G, Olarra A, Yagüe-Fabra JA (2017) Traceability of On-Machine Tool Measurement: A Review, Sensors, 17:1605-1642.

[2] Ostrowska K, Sokal G, Krawczyk M, Kupiec R, Harmatys W, Gaska A, Kowalczyk M, Tomczyk K (2022) Correction of the measuring system composed of the contact probe head mounted on the industrial robot, Measurement, 203: 111957.

[3] Inoue S, Urata A, Kodama T, Huwer T, Maruyama Y, Fujita S, Shinno H, Yoshioka H (2021)-Precision Mobile Robotic Manipulator for Reconfigurable Manufacturing Systems, International Journal of Automation Technology, 15(5): 651-660.

[4] ISO 230-10:2022, Test code for machine tools — Part 10: Determination of the measuring performance of probing systems of numerically controlled machine tools.

[5] Ibaraki S, Theissen NA, Archenti A, Alam MM (2021) Evaluation of Kinematic and Compliance Calibration of Serial Articulated Industrial Manipulators, International Journal of Automation Technology, 15(5): 567-580.

[6] Ostrowska K, Krawczyk M, Kupiec R, Gromczak K, Sladek J (2018) Model of errors of touch-trigger probe installed on the industrial robot, Journal of Physics: Conference Series, 1065(14): 142018.

[7] Denavit J, Hartenberg RS (1955) A kinematic notation for lower-pair mechanisms based on matrices, Journal of Applied Mechanics, 22(2): 215-221.

[8] ISO 230-1:2012, Test code for machine tools -- Part 1: Geometric accuracy of machines operating under no-load or quasi-static conditions.

[9] Zhao N, Ibaraki S (2022) Novel kinematic model of a SCARA-type robot with bi-directional angular positioning deviation of rotary axes, The International Journal of Advanced Manufacturing Technology, 120: 4901-4915

[10] Ibaraki S, Usui R (2022) A novel error mapping of bi-directional angular positioning deviation of rotary axes in a SCARA-type robot by 'open-loop' tracking interferometer measurement, Precision Engineering, 77: 60-68.

[11] Alam MM, Ibaraki S, Fukuda K, Morita S, Usuki H, Otsuki N, Yoshioka H (2022) Inclusion of Bidirectional Angular Positioning Deviations in the Kinematic Model of a Six-DOF Articulated Robot for Static Volumetric Error Compensation, IEEE/ASME Transactions on Mechatronics, 27(6): 4339-4349.

[12] Ibaraki S, Fukuda K, Alam MM, Morita S, Usuki H, Otsuki N, Yoshioka H (2021) Novel six-axis robot kinematic model with axis-to-axis crosstalk, CIRP Annals, 70(1): 411-414.

[13] Ibaraki S, Saito R (2023) Novel kinematic model of articulated arm coordinate measuring machine with angular position measurement errors of rotary axes, CIRP Annals -- Manufacturing Technology, 72(1): 449-452.

[14] Ma L, Bazzoli P, Sammons PM, Landers RG, Bristow DA (2018) Modeling and calibration of high-order joint-dependent kinematic errors for industrial robots, Robotics and Computer-Integrated Manufacturing, 50: 153-167.

[15] Alam MM, Ibaraki S, Fukuda K (2021) Kinematic Modeling of Six-Axis Industrial Robot and its Parameter Identification: A Tutorial, International Journal of Automation Technology, 15(5): 599-610

[16] Ibaraki S, Kawano K (2023) On Thermal Positioning Error of a Planar Robot Arm over Entire Workspace, International Journal of Automation Technology, 17(5):. 504-511